Ensembles of excitable two-state units with delayed feedback

Nikos Kouvaris,[1,2,*] Felix Müller,[1] and Lutz Schimansky-Geier[1]
[1]*Institut für Physik, Humboldt-Universität zu Berlin, Newtonstr. 15, D-12489 Berlin, Germany*
[2]*Institute of Physical Chemistry, National Center for Scientific Research "Demokritos," 15310 Athens, Greece*
(Received 30 June 2010; revised manuscript received 15 October 2010; published 14 December 2010)

A two-state unit is considered as an abstract modification for an excitable system. Each state is characterized by a different waiting time distribution. This non-Markovian approach allows for a renewal process description of the system dynamics. Exact formulas for the interspike interval distribution and power spectral density are found. In the limit of an infinity ensemble of globally coupled units the mean-field equations for the populations of both states are derived. Depending on the coupling strength and on the noise intensity the ensemble undergoes saddle-node bifurcations and demonstrates bistability, while a pitchfork bifurcation emerges on a cusp point. The ensemble undergoes Hopf bifurcations and bulk oscillations emerge, in the onset of coherent activation events, only when the feedback affects individual units with a certain time delay.

DOI: 10.1103/PhysRevE.82.061124 PACS number(s): 02.50.Ey, 02.30.Ks, 87.19.ll, 05.45.Xt

I. INTRODUCTION

The transition to oscillatory behavior from excitable or bistable dynamics is one of the fundamental bifurcations in complex systems. It is a well studied mechanism for single excitable units and for neuronal ensembles [1–3]. There is a various number of neuron models with two or three components including activator and inhibitor dynamics. They describe the voltage and the gating dynamics determining the rest, activation, and refractory states of a neuron. In such continuous models bifurcations emerge by tuning the appropriate control parameters which qualitatively changes the dynamical regimes. The residence times within the steady states corresponding to these dynamical regimes are defined by the interplay of several time scales of the particular model. An additional time scale, that may lead to significant change of common dynamical behaviors in ensembles of coupled neurons, arises due to synaptic and dendritic propagation delays [4–9]. Originally delayed feedback has been proposed to control the dynamics of systems exhibiting deterministic chaos [10]. However it has been also used to control noise-induced dynamics in excitable systems close to a Hopf bifurcation [11–13].

A different approach is the introduction of discrete-states systems where the transitions between the states are modeled by waiting time distributions. This is a successful method applied to study complex stochastic processes [14–17]. In such models where the waiting times are given explicitly, bifurcations can be studied by comparing the time scales in a direct way. Discrete models subjected to delayed feedback exhibit a great variety of dynamical features and a tractable way to control synchrony in neuronal or chemical or other individual based systems [18–23]. A well-known model that consists of two states, can be met in several variations from studies of coherence and stochastic resonance until bifurcation analysis in networks of excitable or bistable units that exhibit oscillatory behavior [17–20].

In this paper a discrete two-state system consisting of a state for a resting phase, and a state corresponding to an excited phase is presented. The novelty of this model lies to its renewal process description. Using appropriate waiting time distributions we investigate the statistical properties of an individual unit and the steady states of a globally coupled ensemble analytically and by numerical simulations. A bistable regime can be found appearing due to saddle-node bifurcations if the coupling includes a feedback that supports activity. When the feedback is delayed an oscillatory regime emerges via a Hopf bifurcation, in the onset of coherent activation and synchronization of coupled units.

II. INDIVIDUAL UNIT

A. Model definition

The system under consideration, depicted in Fig. 1, constitutes a semi-Markovian process for a single unit that changes between two states according to a discrete time Markov chain. However, it spends in each state a random amount of time, distributed by the density functions $w_1(t)$ and $w_2(t)$, respectively.

We construct a renewal process with two discrete states. Although the process is not Markovian, the waiting time in a certain state is independent of the time spent in the preceding state. This single unit aims to mimic a single stochastic excitable system when specific distributions are used. Hence,

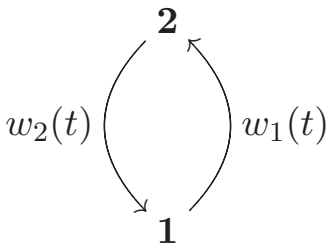

FIG. 1. A two-state excitable unit. State 1 assigns as the resting state, followed by the excited state 2. The waiting times are distributed by an exponential distribution (w_1) in state 1 and by an Erlang distribution (w_2) in state 2.

*Also at Department of Mathematical, Physical and Computational Science, Aristotle University of Thessaloniki, Greece.

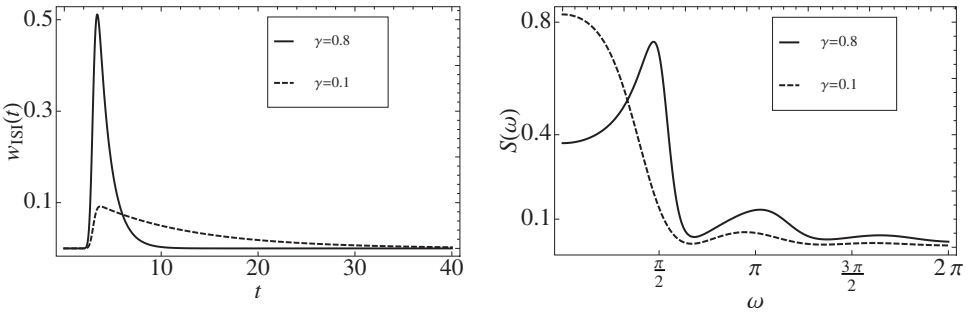

FIG. 2. Left: the interspike interval distribution of a single unit with an exponential (w_1) and an Erlang (w_2) waiting time distribution. Right: the corresponding power spectral density. Parameters $a_2=100$, $t_2=3$. The solid lines show an oscillatory unit, while the dashed lines display excitability.

the transition $1\rightarrow 2$ holds for the activation events while the transition $2\rightarrow 1$ models the return to the rest state. The waiting times in this latter state are distributed by the density function $w_1(t)$ and in the excited state by $w_2(t)$. It is evident that the whole dynamics of such a renewal process is fully specified by the statistical properties of the waiting times between subsequent events. In our system the process is still renewal, however, the distributions of the waiting times will be chosen as different. Thus the waiting times in the resting state obey different statistics than the waiting times in the excited state. The transition $1\rightarrow 2$ is modeled as a rate process,

$$w_1(t) = \gamma \exp(-\gamma t), \tag{1}$$

where both mean and variance equals $1/\gamma$. This is the escape time needed, for an excitable system, to leave the rest state, under the influence of noise. The transition $2\rightarrow 1$ is modeled by an Erlang distribution,

$$w_2(t) = \frac{\alpha_2}{t_2\Gamma(\alpha_2)}\left(\frac{\alpha_2 t}{t_2}\right)^{\alpha_2-1}\exp\left(-\frac{\alpha_2 t}{t_2}\right), \tag{2}$$

where α_2 is integer. The mean value equals t_2 and the variance t_2^2/α_2. This distribution describes the waiting time in the excited state corresponding to the quasideterministic spike production when the impact of fluctuations is negligible. Therefore the width of w_2 has to be narrow, realized by choosing large values of α_2 where the Erlang distribution is close to a δ-distribution. The choice of w_1 and w_2 results from the basic features of excitable systems, which have a stable fixed point. By noise, they can escape from that fixed point with a certain randomly distributed time, modeled by w_1. The following excursion in phase space is less affected by noise, however, the time can also vary with a small dispersion. This motivates us to the assumption for our model that the resting state corresponds to the fixed point and the excited state to the excursion in the phase space.

B. Interspike interval distribution and power spectral density

The renewal process describes the system above gives rise to a stochastic pulse sequence defined as $s(t)=0$ in the resting state and $s(t)=1$ in the excited. Analyzing its statistical properties, characteristic features of excitable systems can be extracted.

The interspike interval (ISI) is the sequence of excitation time followed by the activation time. Employing the renewal theory, the ISI distribution can be expressed as the convolution of their waiting time density functions [see Fig. 2 (left)],

$$w_{ISI}(t) = \gamma \exp(-\gamma t)\left(\frac{a_2}{a_2-\gamma t_2}\right)^{a_2} \times\left[1-\frac{\Gamma(a_2,(a_2/t_2-\gamma)t)}{\Gamma(a_2)}\right]. \tag{3}$$

The corresponding power spectral density (PSD) of the pulse sequence $s(t)$ is shown in Fig. 2 (right). It can be expressed in terms of the corresponding waiting time densities [14,24] and is given by the formula

$$S(\omega) = \frac{4}{\omega^2(t_2+1/\gamma)}\mathrm{Re}\frac{\omega[(1-i\omega t_2/a_2)^{a_2}-1]}{(\omega+i\gamma)(1-i\omega t_2/a_2)^{a_2}-i\gamma}. \tag{4}$$

When $1/\gamma \gg t_2$ (dashed lines in Fig. 2) the unit spends more time in the resting state and the ISI distribution is broad. Otherwise, if $1/\gamma \ll t_2$ (solid lines in Fig. 2) the unit behaves like an oscillator between the two states with a spectral maximum at finite nonzero frequencies. The corresponding ISI are narrow distributed around the mean period of one cycle ($T=1/\gamma+t_2$). Both PSD and ISI give evidence to coherence resonance, as there are some preferable frequencies that increase the pulse regularity [25–28].

C. Generalized master equations

The balance of probability flows serves to determine the occupation probabilities $P_i(t)$, $i=1,2$ of separate states i. The generalized master equations [29] that hold for these probabilities read

$$\frac{d}{dt}P_1(t) = -J_{1\rightarrow 2}(t) + J_{2\rightarrow 1}(t), \tag{5a}$$

$$\frac{d}{dt}P_2(t) = -J_{2\rightarrow 1}(t) + J_{1\rightarrow 2}(t), \tag{5b}$$

where $J_{1\rightarrow 2}(t)$ and $J_{2\rightarrow 1}(t)$ denote the probability flow from state 1 to 2 at time t and vice versa. Since the transition $1\rightarrow 2$ is a rate process, its probability flow is given by $J_{1\rightarrow 2}(t)=\gamma P_1(t)$. The second probability flow is given by the product of $J_{1\rightarrow 2}$ at $t-t'$ with the probability density $w_2(t')$ to wait in state 2 the time t', integrated for all possible t', namely $J_{2\rightarrow 1}(t)=\int_0^\infty \gamma P_1(t-t')w_2(t')dt'$. Then Eq. (5b) reads

$$\frac{d}{dt}P_2(t) = \gamma P_1(t) - \int_0^\infty \gamma P_1(t-t')w_2(t')dt'. \tag{6}$$

The Eq. (6) supplemented by the normalization condition

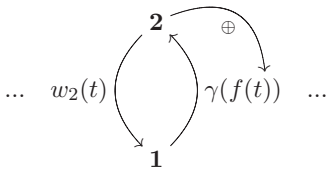

FIG. 3. Ensemble of globally coupled units by their global output $f(t)$.

$$P_1(t) = 1 - P_2(t), \tag{7}$$

can be given in the closed form

$$\frac{d}{dt}P_2(t) = \gamma[1 - P_2(t)] - \int_0^\infty \gamma[1 - P_2(t-t')]w_2(t')dt'. \tag{8}$$

This integrodifferential Eq. (8) has to be supplemented by initial conditions obeying normalization and contains all the dynamical features of a single unit.

III. ENSEMBLES OF COUPLED UNITS

A. Global coupling

The collective behavior of a large population of interconnected two-state units, illustrated in Fig. 3, results from the interplay of individual participants. In order to investigate its dynamics, an ensemble of N units coupled by their global output $f(t)$, is considered. By this coupling the information transmitted to each unit is the fraction of excited units of the ensemble. Although the characteristics of the waiting time densities do not change due to coupling, the activation rate γ depends on $f(t)$. This mechanism can be expressed by the sum of output of all units

$$f(t) = \frac{1}{N}\sum_{j=1}^{N} s_j(t) = \frac{n_2(t)}{N}, \tag{9}$$

where $n_2(t)$ is the fraction of units in the excited state at time t. Obviously, $f(t)$ equals the relative occupation number of the excited state. Assuming $P_N(n_2,t)$ to be the probability to find n_2 units in state 2 at time t and considering the continuum limit of infinitely many coupled units $N\to\infty$, $f(t)$ converges to P_2 [30],

$$\lim_{N\to\infty} f(t) = P_2(t). \tag{10}$$

We thus consider the activation rate as a function of $P_2(t)$,

$$\gamma = \gamma[P_2(t)], \tag{11}$$

and the same for all the units. The equation that governs the collective dynamics of the ensemble is uniquely determined by the Eq. (8) for occupation probabilities of individual units. To that end, by taking Eq. (11) into account, the mean-field (MF) equation reads,

$$\frac{d}{dt}P_2(t) = \gamma[P_2(t)][1 - P_2(t)] - \int_0^\infty \gamma[P_2(t-t')][1 - P_2(t-t')]w_2(t')dt'. \tag{12}$$

In general, Eq. (11) induces an implicit form of steady state solution, which can be expressed as

$$P_2^* = \frac{t_2}{1/\gamma(P_2^*) + t_2}. \tag{13}$$

The complementary steady state comes from the normalization condition $P_1^* = 1 - P_2^*$. Adding small perturbations $P_i(t) = P_i^* + a_i \exp(\lambda t)$ into the linearized MF-equation, the linear stability of its steady state can be acquired. Therefore the characteristic equation for the eigenvalues is formulated as

$$\lambda + \left[\gamma(P_2^*) - \frac{d\gamma(P_2^*)}{dP_2^*}(1 - P_2^*)\right][1 - \hat{w}_2(\lambda)] = 0, \tag{14}$$

where $\hat{w}_2(\lambda)$ is the Laplace transform of $w_2(t)$. It can be shown that the eigenvalues λ can never be purely imaginary. That means no Hopf bifurcation exists. However, an appropriate choice for the dependence of γ on $P_2(t)$ can introduce strong nonlinearities into the Eq. (12).

In the following an Arrhenius law is assumed for the activation rate. Instabilities come into the system by the adoption of excitatory coupling, namely, γ has to be an increasing function of P_2,

$$\gamma[P_2(t)] = r_0 \exp\left\{-\frac{\Delta U_0}{D}[1 - \sigma P_2(t)]\right\}, \tag{15}$$

where ΔU_0 is an activation constant, D is the noise intensity and σ is the coupling strength. This adoption fulfills the conditions for Kramer's time $(1/\gamma)$ when D is sufficiently low. It has been used in studies of coherent and stochastic resonance [26,28] and in globally coupled networks of bistable elements [14,19,31].

This excitatory feedback is not able to destabilize the units from the resting state when the coupling σ is sufficiently small, as shown in Fig. 4 (left). This steady state is linear stable, the activation time is very long and the majority of units lies to the resting state. Following this stable branch for intermediate σ a bistable regime appears. The system comes into this regime through a saddle-node bifurcation when the slopes of both sides of Eq. (13) become equal. In other words reaching for the first time the curve, given by

$$\frac{\Delta U_0}{D}(\sigma P_2^* - 1) = \log\left(\frac{\Delta U_0 \sigma P_2^* - D}{r_0 D t_2}\right), \tag{16}$$

one of the real eigenvalues vanishes and two new fixed points appear, an unstable and a stable one. Increasing σ further, the first stable point merges with the unstable and collapse onto a second saddle-node bifurcation. Eventually, the system leaves bistability and only the upper branch survives, where the majority of units are excited. The whole

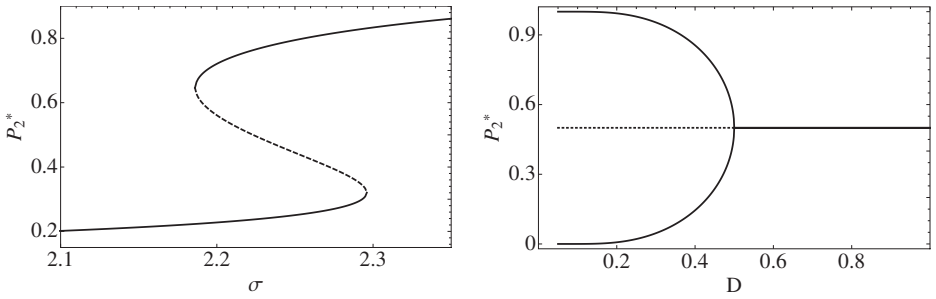

FIG. 4. Bifurcation diagrams of stationary steady state P_2^*. Left: saddle-node bifurcations with respect to coupling strength ($D=0.5$). Right: pitchfork bifurcation with respect to noise intensity ($\sigma=2$). The other parameters are $a_2=100, t_2=1$, $r_0=0.8$, and $\Delta U_0=1$.

scenario is illustrated in the bifurcation diagram Fig. 4 (left) and by the insets of Fig. 5. It is important to note here that although this upper branch is stable, a unit can leave this steady state after its individual excitation time. Nevertheless, it reaches the branch again after a vanishing short activation time.

The system alternates dynamical regimes also due to noise intensity. At low noise level it exhibits bistability [Fig. 4 (right)]. However, for larger values of D it ends up to single steady state, where the units are equally distributed between both states. If additionally the second derivative of Eq. (13) vanishes at $P_2=P_2^*$ both stable branches merge in a cusp point,

$$\sigma^{\text{cusp}} = \frac{4D^{\text{cusp}}}{\Delta U_0}, \quad D^{\text{cusp}} = \frac{\Delta U_0}{2+\log(r_0 t_2)}, \tag{17}$$

where a supercritical pitchfork bifurcation takes place. Under this symmetry breaking, two stable fixed points disappear, while the middle one gains its stability. The dynamical regimes and the cusp point are shown on $D-\sigma$ parameter plane in Fig. 5. Both folds that define saddle-node bifurcations merge in this cusp point and the bistability vanishes. A geometric sketch of the left and the right hand side of Eq. (13) are shown as insets in the same figure in order to identify the different dynamical regimes. Note, that the single elements still change between resting and excited state following their individual waiting time distributions. However the ensemble reaches one of two states, determined by the system parameters and the initial configuration of units distributed in both states.

Let us note that neglecting the refractory state in the three-state model [14,30] it converges to our two-state model without delayed coupling. However, the bifurcation analysis presented above reveals all the details that describe the different behavior observed in the two stable branches, which results from the internal clock of units. Similar behavior should be observed in the cited three-states system.

B. Global delayed coupling

Up to this point the global output feds back immediately to the rate γ. However, due to finite propagating velocity of information in networks of individual participants (like neuronal networks), we assume a feedback that needs a certain but fixed delay time τ to act on individual elements. This coupling mechanism induces significant variations in the coupled two-state units. It can improve the coherence properties and change drastically the underlying dynamics.

In the same manner like before, the rate γ is assumed as an increasing function of $P_2(t-\tau)$, meaning that the activation time strongly depends on the fraction of units that were excited at a fixed time delay τ. The MF-equation now reads

$$\frac{d}{dt}P_2(t) = \gamma[P_2(t-\tau)][1-P_2(t)] - \int_0^\infty \gamma[P_2(t-t'-\tau)][1-P_2(t-t')]w_2(t')dt'. \tag{18}$$

A prefactor $\exp(-\lambda\tau)$ comes into the characteristic equation for the eigenvalues,

$$\lambda + \left[\gamma(P_2^*) - \frac{d\gamma(P_2^*)}{dP_2^*}(1-P_2^*)\exp(-\lambda\tau)\right][1-\hat{w}_2(\lambda)] = 0 \tag{19}$$

and has crucial influence on the system linear stability [32]. For a given set of parameters the delayed feedback gives rise to Hopf bifurcations, since Eq. (19) has complex solutions that pass simultaneously the imaginary axis.

In the following, fluctuations in the excited state are completely neglected. Therefore, by setting $\alpha_2 \to \infty$ the transition $2 \to 1$ has a fixed time t_2, namely, $w_2(t)=\delta(t-t_2)$. Hence, its

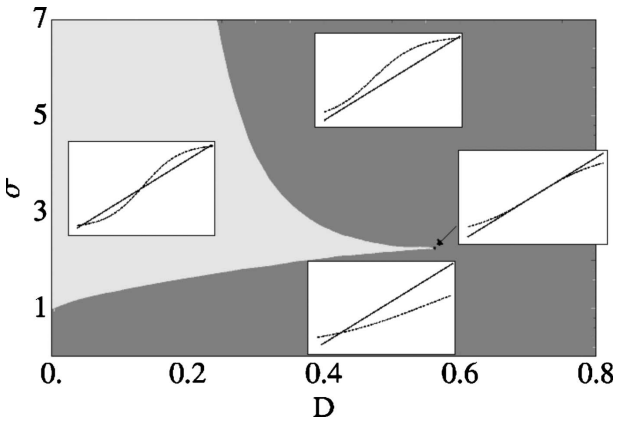

FIG. 5. Stability diagram on $D-\sigma$ plane. The monostable regime is shown in dark gray, while light gray corresponds to the bistable regime. On the borders of two regimes saddle-node bifurcations take place, while a pitchfork bifurcation emerges in the cusp point (black color). The insets in the corresponding regimes, show geometrically the stationary states P_2^* from Eq. (13). The remaining parameters are the same as in Fig. 4.

Laplace transform is $\hat{w}_2(\lambda)=\exp(\lambda t_2)$. By taking this into account it finally gives the classical form of a characteristic equation with two delays:

$$\lambda + \left[\gamma(P_2^*) - \frac{d\gamma(P_2^*)}{dP_2^*}(1-P_2^*)\exp(-\lambda\tau) \right][1-\exp(-\lambda t_2)] = 0. \tag{20}$$

Setting $\lambda=\imath\omega$ and separating Eq. (20) into real and imaginary part the Hopf bifurcations in the plane $D-\sigma$ are given by the parametric curve

$$D_H = \frac{2\Delta U_0}{2\log\left\{\frac{\omega}{2r_0}[\cot(\omega\tau)+\cot(\omega t_2/2)]\right\} - \frac{\omega t_2}{\sin(\omega\tau)}}, \tag{21a}$$

$$\sigma_H = \frac{t_2 D_H}{2\Delta U_0 P_2^*}\frac{\omega}{\sin(\omega\tau)}, \tag{21b}$$

where ω stands for the frequencies of critical oscillations on the bifurcation curve [see Fig. 6 (inset)]. The location of this curve depends on time delay and divides the $D-\sigma$ plane in two dynamical regimes, the oscillating and the nonoscillating domains, as illustrated in Fig. 6. Inside the oscillating regime all units undergo the transitions $1\to2\to1$ in a coherent way leading to an oscillatory global output. Out of this area, although all units change between both states following their individual waiting time distributions, the ensemble ends up to a stationary state and exhibits no rhythmic phenomena.

There is a minimum delay below which no Hopf bifurcation emerges. An analytical approximation of this critical delay is calculated geometrically close to the solution of Eq. (21b), when it has only one solution with respect to ω. This estimation gives,

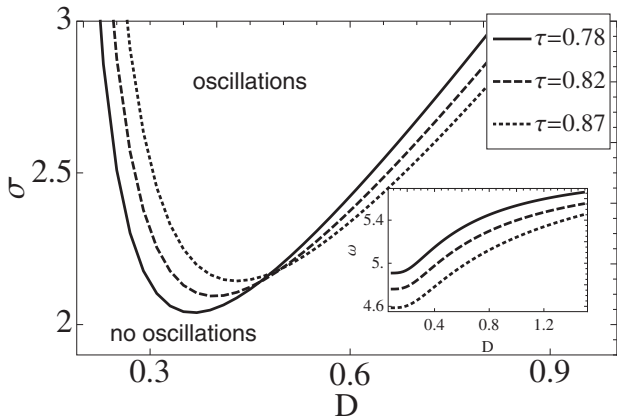

FIG. 6. The curves show parameters where a Hopf bifurcation takes place in the parametric plane $D-\sigma$ for different delays. The corresponding frequencies on bifurcation points are shown in the inset. The parameters are fixed at $t_2=1$, $r_0=0.8$, and $\Delta U_0=1$.

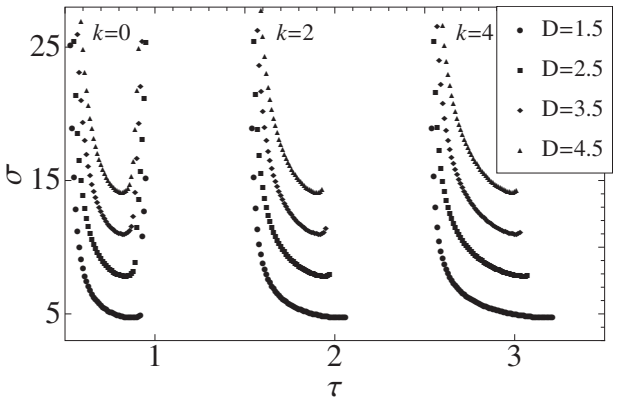

FIG. 7. Reappearance of primary branch ($k=0$) of Hopf bifurcations for larger delays. Some parts are squeezed and some parts are stretched, depending on their frequency ω. The remaining parameters are the same as in Fig. 6.

$$\tau^{\text{critical}} \approx \frac{3\pi}{4}\frac{t_2 D}{\sigma\Delta U_0 P_2^*}. \tag{22}$$

This critical value defines the position of the primary branch in Fig. 7.

From the parametric Eqs. (21) for the Hopf bifurcation points, additional solutions can be easily derived, given by,

$$\tau' = \tau + \frac{k\pi}{\omega}, \tag{23}$$

where $k=0,1,2\ldots$. Equation (23) indicates reappearance of Hopf bifurcations and periodic solutions for larger delays. The primary branch of these solutions appears at finite delays for $k=0$ as shown in Fig. 7. The reappearance of this primary branch for larger delays ($k=2,4,\ldots$) is also shown in the same figure. These branches have the same frequency dependence, since they consist of the same periodic solutions (for even values of k), however with some stretchings and squeezings. Let us assume two solutions with different frequencies for delays τ_1 and τ_2, with $\tau_1<\tau_2$, on the primary branch. The projection of their distance on τ axis is defined as

$$\ell = \tau_2 - \tau_1. \tag{24}$$

The distance of the same solutions on the kth branch is given by using Eq. (23) as

$$\ell' = \tau_2' - \tau_1' = \ell + k\pi\frac{\omega_1-\omega_2}{\omega_1\omega_2}. \tag{25}$$

From Eq. (25) it is clear that $\ell'>\ell$ when $\omega_1>\omega_2$ and thus the corresponding parts of kth branch will be stretched, otherwise they will be squeezed. This seems to be a general behavior of delayed system with periodic solutions [33]. Finally, from Eq. (23) follows that $\sin(\omega\tau)=-\sin(\omega\tau')$ for odd values of k, which is a solution of Eq. (21a) when σ_H is negative. Therefore, the system undergo a Hopf bifurcation for inhibitory coupling ($\sigma<0$) with τ', however, for different values of noise intensity.

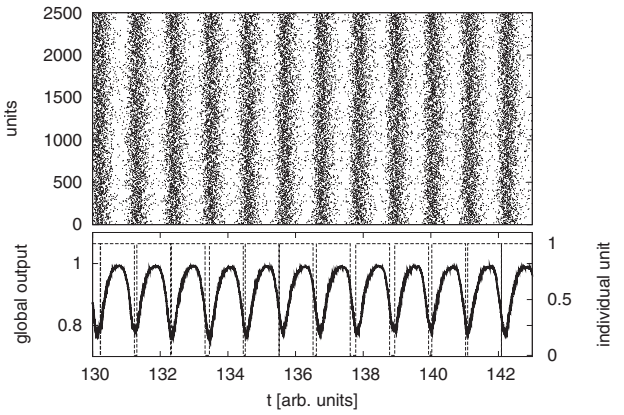

FIG. 8. Top: record of the activity of 2500 units with delayed global coupling. Black dots stand for the moments where transition $1 \rightarrow 2$ starts. Bottom: the output of an arbitrary chosen unit (thin dashed line) and the oscillatory global output (thick solid line). The parameters in this simulation are chosen as $\tau=0.78, D=0.49, \sigma=2.5$.

IV. NUMERICAL SIMULATIONS

The dynamics of a global coupled chain constituted of a large number of two-state units is simulated in order to verify the theory presented above. We consider a large ensemble of such coupled units, which comes closer to the mean-field dynamics the larger the ensemble is. Each individual unit has its own internal clock defined by the distributions w_1 and w_2. The time resolution (time step) is chosen to be $dt=10^{-7}$ and the simulation runs for 200×10^7 time steps. Each time an individual unit starts the transition $1 \rightarrow 2$, a random amount of time is chosen to be exponentially distributed by w_1 for the activation time of that unit. In the first case, the rate γ of w_1 is affected by the current global output $f(t)$ of the whole ensemble, while the excitation times follows the Erlang distribution w_2. In the case of delayed feedback, γ is affected by the global output $f(t-\tau)$ of the ensemble in a previous time $t-\tau$, while the excitation time is constant (t_2).

In the absence of delayed feedback and with an Erlang distribution for the waiting times in the excited state, monostable or bistable behavior is observed. In the bistable case one of the stationary states can be selected by choosing appropriate initial configurations. Note, that the individual units behave in a different way along the two stable branches, as already mentioned for the infinity system at the MF level. For occupation probabilities within the lower stable branch the activation time can be very long. Therefore the majority of units are staying longer in the resting state. The behavior is different in the upper branch. Although it is stable, each unit transit to the resting state after a finite excitation time. Nevertheless, it becomes excited again after a vanishing short activation time. This complex behavior arises because the single elements always change between two states following their individual internal clocks.

By applying the delayed feedback and assuming a constant excitation time, an additional time scale is introduced that can result to bulk oscillations, presented in Fig. 8. As predicted in the theory the oscillating regime occurs for parameters D and σ beyond the Hopf line given by the Eqs. (21). In the upper panel of Fig. 8 the activity of 2500 units coupled by delayed feedback is recorded, where the black dots mark the transition events to the excited state. The activity of an arbitrary chosen individual unit (dashed line) and the global output (solid line) are depicted in the lower panel. The majority of units subjected to transitions between states within the same time interval, manifesting synchronization of the units and therefore coherent activation of the coupled chain. A parameter scan along the D and σ axis in Fig. 6 crossing the Hopf line is shown in Figs. 9 and 10 for two measures of coherent global oscillations. Let us mention here that we use these measurements only to figure out the bifurcation point in simulations and to characterize the coherence properties very close to the Hopf line. They give correct results only for small values of σ and D where the Arrhenius law is satisfied.

The very presence of oscillations as illustrated in Fig. 8 can be captured by the quantification of an amplitude in the global output using its variance $\langle f(t)-\langle f(t)\rangle\rangle^2$. This quantity takes nonzero values as soon as the Hopf-line is exceeded by a smooth increase over D and rises abruptly over σ. The degree of coherence close to the Hopf bifurcation can be characterized by the synchronization index (SI). Following the analytic signal approach [34] of a measured signal $z(t)$, which is the global output in our case, one can define

$$\zeta(t) = z(t) + i\tilde{z}(t) = A(t)e^{i\phi(t)}, \tag{26}$$

where the imaginary part $\tilde{z}(t)$ is the Hilbert transform of $z(t)$. The instantaneous phase $\phi(t)$ of the signal is uniquely defined by Eq. (26). Assuming two arbitrary chosen subensembles, each consisting of 50 units, the phase difference between them is defined as, $\Delta\phi=\phi_1(t)-\phi_2(t)$. Therefore the SI can be estimated, given by

$$\text{S.I.} = \langle\cos(\Delta\phi)\rangle^2 + \langle\sin(\Delta\phi)\rangle^2, \tag{27}$$

which relates in Gaussian approximation to the variance of $\Delta\phi$ distribution. When phases are narrow distributed around a constant value SI goes to unity, otherwise for broad distributed phases it goes to zero. In Figs. 9 and 10 it can be seen,

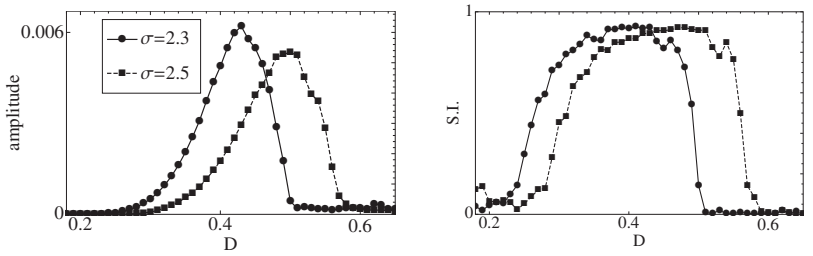

FIG. 9. Oscillations amplitude (left) and synchronization index (right) with respect to noise intensity.

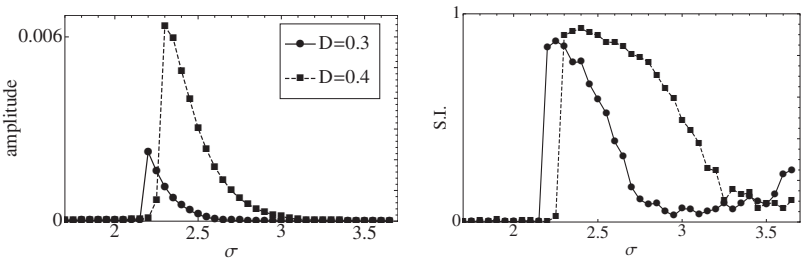

FIG. 10. Oscillations amplitude (left) and synchronization index (right) with respect to coupling strength.

that the SI grows at the Hopf values similar to the amplitude and shows a pronounced synchronization maximum. Coming closer the second Hopf-bifurcation point by further increase of noise intensity D both measures decrease to zero. For higher σ there is no second Hopf bifurcation (see Fig. 6). However, the amplitude as well as the SI shrinks after passing the maximum. This lessening can be explained by considering the interplay of time scales. The activation rate becomes greater with higher coupling, so the mean activation time $1/\gamma$ becomes very short and most units occupy the excited state in the same time. Although the individual units keep rotating between two states, they spend vanishing short time in the resting state. Because of the finite size of chain, the global output practically does not affected by these transitions and finally seems to be not oscillatory, deluding both measurements, amplitude and synchronization index, which are assumed only for oscillatory signals. However for small D and σ, they give the bifurcation point adequately close to the mean-field theory and they found increase of coherence close to bifurcation. This behavior of very short activation time, which stabilizes the depolarized state, is indeed known from neurobiology. The occurrence of a stable depolarized state often corresponds to a pathological regime of neuronal behavior, such as spreading depression [35] or poisoning of cells by potassium [36,37]. In these studies, due to synaptic or intercellular chemical coupling, the excitable units perform a delayed interaction due to finite propagation velocity. If this effect is strong enough, they show a bursting behavior and even more, a regime of almost complete depolarization over a long time.

V. CONCLUSIONS

Analytical studies and simulations results indicate that large ensembles of coupled two-state units exhibit a rich dynamics. At the MF level, global excitatory coupling leads to monostability and bistability, which alternate through saddle-node or pitchfork bifurcations. Each unit changes between both states following its individual waiting time distribution. The latter nevertheless is affected by the global coupling driving the ensemble to one of two dynamical regimes. It is important to note that although the ensemble reaches one of the two stable steady states, the individual units still transit between excited and resting state, following their internal clock. A more complex behavior arises, when global coupling feds back to each individual activation time after a certain time delay. The ensemble now passes through a Hopf bifurcation to an oscillating regime, in the sense of almost synchronous activation. For appropriate time delay a Hopf bifurcation occurs for inhibitory coupling, however for different values of noise intensity. Future work is necessary to develop a locally coupled model in order to investigate spatial behavior in the various dynamical regimes.

ACKNOWLEDGMENTS

The authors acknowledge support by DFG Sfb555 and the Bernstein Center for "Computational Neuroscience Berlin." N.K. and F.M. thank A. Provata, M. Zaks, S. Rüdiger and S. Yanchuck for fruitful discussions.

[1] E. M. Izhikevich, Int. J. Bifurcation Chaos Appl. Sci. Eng. **10**, 1171 (2000).
[2] E. Ullner, A. Zaikin, J. García-Ojalvo, and J. Kurths, Phys. Rev. Lett. **91**, 180601 (2003).
[3] V. S. Anishchenko, V. Astakhov, A. Neiman, T. Vadivasova, and L. Schimansky-Geier, *Nonlinear Dynamics of Chaotic and Stochastic Systems* (Springer, Berlin, 2007).
[4] M. A. Dahlem, G. Hiller, A. Panchuk, and E. Schöll, Int. J. Bifurcation Chaos Appl. Sci. Eng. **19**, 745 (2009).
[5] F. M. Atay and A. Hutt, SIAM J. Appl. Dyn. Syst. **5**, 670 (2006).
[6] M. Dhamala, V. K. Jirsa, and M. Ding, Phys. Rev. Lett. **92**, 074104 (2004).
[7] H. Haken, *Brain Dynamics: Synchronization and Activity Patterns in Pulse-Coupled Neural Nets with Delays and Noise* (Springer, Berlin, 2006).
[8] H. R. Wilson, *Spikes, Decisions, and Actions: The Dynamical Foundations of Neuroscience* (Oxford University Press, Oxford, UK, 1999).
[9] O. V. Popovych, C. Hauptmann, and P. A. Tass, Biol. Cybern. **95**, 69 (2006).
[10] *Handbook of Chaos Control*, edited by E. Schöll and H. G. Schuster (Wiley-VCH, Weinheim, 2008).
[11] N. B. Janson, A. G. Balanov, and E. Schöll, Phys. Rev. Lett. **93**, 010601 (2004).
[12] A. G. Balanov, N. B. Janson, and E. Schöll, Physica D **199**, 1 (2004).
[13] B. Hauschildt, N. B. Janson, A. G. Balanov, and E. Schöll, Phys. Rev. E **74**, 051906 (2006).
[14] T. Prager, B. Naundorf, and L. Schimansky-Geier, Physica A

325, 176 (2003).
[15] K. Wood, C. Van den Broeck, R. Kawai, and K. Lindenberg, Phys. Rev. E **74**, 031113 (2006).
[16] T. Schwalger and B. Lindner, Phys. Rev. E **78**, 021121 (2008).
[17] B. McNamara and K. Wiesenfeld, Phys. Rev. A **39**, 4854 (1989).
[18] T. Ohira and T. Yamane, Phys. Rev. E **61**, 1247 (2000).
[19] D. Huber and L. S. Tsimring, Phys. Rev. Lett. **91**, 260601 (2003); Phys. Rev. E **71**, 036150 (2005).
[20] M. Kimizuka and T. Munakata, Phys. Rev. E **80**, 021139 (2009).
[21] T. Prager, H. P. Lerch, L. Schimansky-Geier, and E. Schöll, J. Phys. A **40**, 11045 (2007).
[22] M. K. Stephen Yeung and S. H. Strogatz, Phys. Rev. Lett. **82**, 648 (1999).
[23] S. Trimper and K. Zabrocki, Phys. Lett. A **321**, 205 (2004).
[24] R. L. Stratonovich, *Topics in the Theory of Random Noise I* (Gordon and Breach, New York, 1962).
[25] L. Gammaitoni, P. Hänggi, P. Jung, and F. Marchesoni, Rev. Mod. Phys. **70**, 223 (1998).
[26] A. S. Pikovsky and J. Kurths, Phys. Rev. Lett. **78**, 775 (1997).
[27] B. Lindner and L. Schimansky-Geier, Phys. Rev. E **61**, 6103 (2000).
[28] T. Prager and L. Schimansky-Geier, Phys. Rev. Lett. **91**, 230601 (2003).
[29] V. M. Kenkre, E. W. Montroll, and M. F. Schlesinger, J. Stat. Phys. **9**, 45 (1973); D. T. Gillespie, Phys. Lett. A **64**, 22 (1977).
[30] T. Prager, M. Falcke, L. Schimansky-Geier, and M. A. Zaks, Phys. Rev. E **76**, 011118 (2007).
[31] P. Jung, U. Behn, E. Pantazelou, and F. Moss, Phys. Rev. A **46**, R1709 (1992).
[32] G. T. Gurija and M. A. Livshits, Z. Phys. B: Condens. Matter **47**, 71 (1982).
[33] S. Yanchuk and P. Perlikowski, Phys. Rev. E **79**, 046221 (2009).
[34] A. S. Pikovsky, M. G. Rosenblum, and J. Kurths, *Synchronization, a Universal Concept in Nonlinear Science* (Cambridge University Press, Cambridge, England, 2001).
[35] M. A. Dahlem and S. C. Muller, Ann. Phys. **13**, 442 (2004).
[36] F. Fröhlich, M. Bazhenov, V. Iragui-Madoz, and T. J. Sejnowski, Neuroscientist **14**, 422 (2008).
[37] D. E. Postnov, F. Müller, R. B. Schuppner, and L. Schimansky-Geier, Phys. Rev. E **80**, 031921 (2009).